https://doi.org/10.1016/j.measurement.2020.108646

Power Compensation Mechanism for AMB System in Magnetically Suspended Flywheel Energy Storage System

Biao Xiang and Waion Wong

Department of Mechanical Engineering, Hong Kong Polytechnic University, Kowloon, Hong Kong SAR, China

Abstract

The active magnetic bearing (AMB) system is the core part of magnetically suspended flywheel energy storage system (FESS) to suspend flywheel (FW) rotor at the equilibrium point, but the AMB system needs power supply system to suspend FW rotor. The stable suspension of FW rotor cannot be guaranteed if the on-board power supply system fails to work, so the unstable FW rotor causes fatal damage to magnetically suspended FESS. Therefore, an off-board power supply system is designed to maintain the stable suspension of FW rotor when the on-board power supply system fails to work. Simultaneously, the dynamic braking of FW rotor is realized by discharge of magnetically suspended FESS, so dynamic displacements of FW rotor are kept at equilibrium status. Simulation and experiment are conducted to verify that the off-board power supply system timely restores AMB system, and dynamic displacements of FW rotor are timely returned to the equilibrium point.

***Keywords*—active magnetic bearing；magnetically suspended flywheel energy storage system；flywheel rotor；discharge；dynamic displacements.**

I. INTRODUCTION

The flywheel energy storage system (FESS) [1] is a complex electromechanical device for storing and transferring mechanical energy to/from a flywheel (FW) rotor by an integrated motor/generator system [2, 3]. The FESS storages the mechanical energy as a motor system through accelerating or maintaining high rotational speed, and outputs the mechanical energy as a generator by decelerating the rotational speed. The FESS was used in the uninterruptable power supply (UPS) system [4], the isolated hybrid grid in renewable energy system [5], the voltage transmission system between offshore wind farm and onshore grid [6-8], the power system in land vehicle [9] and the space power battery system [10] because the FESS has advantages of high cycle life, long operational life, high round-trip efficiency, high power density and low environmental impact [11]. Furthermore, in order to improve the energy storage capacity and the active vibration controllability of FESS, the active magnetic bearing (AMB) system is applied in the FESS to suspend the FW rotor at the equilibrium position [12-14]. On the one hand, the friction between stator part and rotor part of the FESS would be eliminated by suspending the FW rotor at the equilibrium location, so the power loss caused by the mechanical friction could be reduced, and the rotational speed would be increased [15-17]. On the other hand, based on the displacement feedback of FW rotor, the vibration of FW rotor could be controlled when it works at different rotational speeds by tuning the magnetic forces of AMB system [18-20].

In the magnetically suspended FESS, the AMB system is the most critical part to ensure the stable transformation of FW rotor between the charge state and the discharge state. Therefore, the stability and security of AMB system are the important elements for the magnetically suspended FESS during the operational status. However, the sudden power failure of AMB system perhaps cause fatal damage to the magnetically suspended FESS [21, 22], especially when the

FW rotor works at a high rotational speed. The collisions of main rotational spindle unit were investigated, and collision damages of the developed spindle system under normal process conditions as well as in collision situations were proved in various experiments [23]. Moreover, the rotor system was easily subjected to rapid increase of the unbalance term, and then the high contact force between rotor part and stator part caused possible catastrophic failure to the whole rotor system [24].

Therefore, the power compensation mechanism for AMB system should be applied in the magnetically suspended FESS. In the meanwhile, the FESS could output the stable direct-current (DC) voltage in the discharge process [25-28], so the discharge process of magnetically suspended FESS is a suitable and reliable option to provide the additional power supply to AMB system in case of a sudden failure of the on-board power supply system. Moreover, the switch time interval between the charge process and the discharge process of FESS is about micro second [29], so it could satisfy the requirement on the fast response of discharge system.

In this article, the charge and discharge strategies of magnetically suspended FESS are investigated. As illustrated in Fig. 1, when the on-board power supply system fails to work, the supplementary off-board power supply system of AMB system based on the discharge of magnetically suspended FESS is designed to be an optional power supply system for the AMB system. During the charge process of magnetically suspended FESS, the sliding mode control (SMC) is designed to regulate the q-axis voltage of magnetically suspended FESS, and the voltage of AMB system is timely measured by the voltage sensor and fed back to MCU on board. In case of failure of on-board power supply system, the discharge process of magnetically suspended FESS could be realized by three-phase rectification technology, and then the discharge voltage would be transformed into the off-board power supply by voltage transformation technology. Therefore, the power compensation of AMB system could be successfully realized.

This article is organized as follows, the structure and principle of magnetically suspended FESS including charge/discharge system, DC/DC converting module and AMB system are introduced in section II. The simulations about the discharge/charge processes of magnetically suspended FESS are conducted in section III. The experiments about the power compensation of magnetically suspended FESS are designed to verify the effectiveness of proposed method in section IV. Finally, the conclusions are summarized.

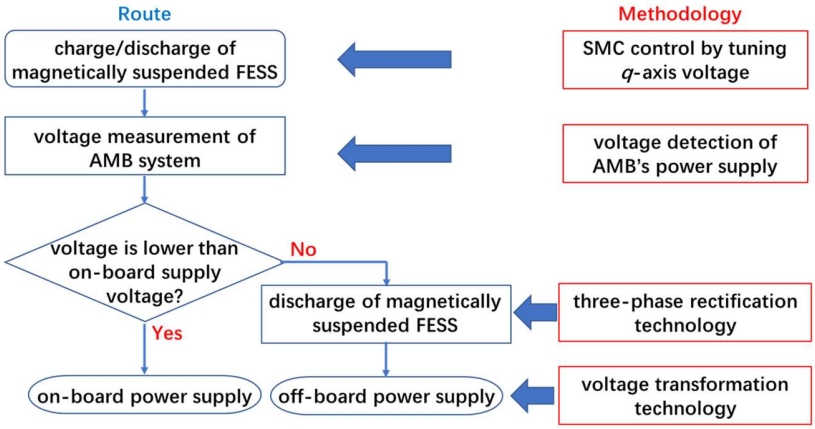

Fig. 1. The process of power compensation for AMB system in magnetically suspended FESS.

II. STRUCTURE OF MAGNETICALLY SUSPENDED FESS

A. Charge/Discharge System

The magnetically suspended FESS shown in Fig. 2 includes a charge/discharge module of magnetically suspended FESS and a control module of AMB system. The charge/discharge module of magnetically suspended FESS in the blue block diagram contains a FW rotor, a three-phase driving unit and a main control unit (MCU). The FW rotor could be used in an integrated motor/generator with different control models, and it outputs the DC voltage through rectifying the back electromotive force (EMF) with the reference input DC voltage. The three-phase driving unit includes a space vector (SV) switch table, a plus width modulation (PWM) generator and a three-phase invertor. The SV switch table generates switch signal based on the α-axis and β-axis input currents. In addition, the control scheme of MCU has two different control loops including a q-axis control loop and a d-axis control loop. For the q-axis control loop, the proportional-integral (PI) controller generates the q-axis input current based on the voltage feedback in the external control loop, and then the inner control loop generates the q-axis input voltage. For the d-axis control loop, the PI controller realizes the closed-loop control based on the d-axis feedback current.

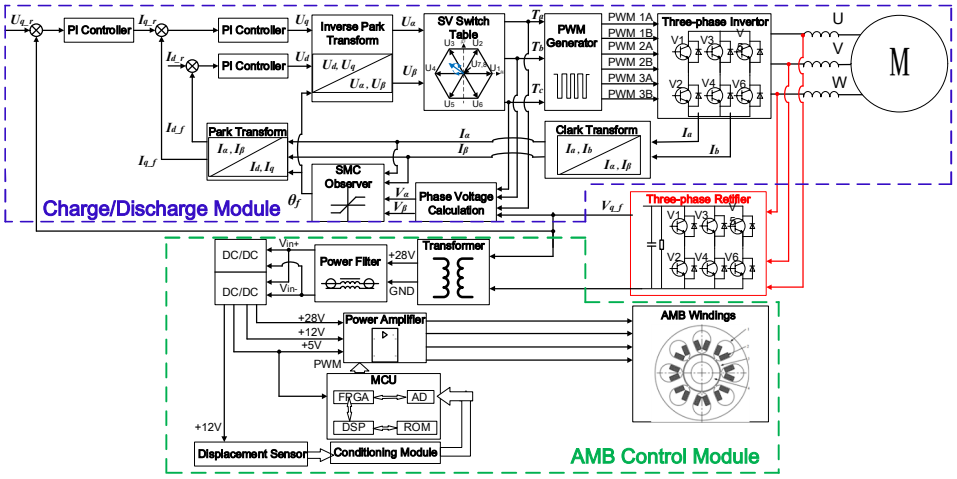

Fig. 2. The scheme of whole charge/discharge mechanism.

The control module of AMB system in the green block diagram has an MCU, a driving unit and a measurement unit. The MCU based on a digital signal processor (DSP) chip and a field-programmable gate array (FPGA) chip generates the control signal to the driving unit of AMB system. The driving unit outputs the control current to drive the AMB system which has two different modules. During the normal operation, the power supply is provided by the on-board power supply system through the voltage transformer and the DC/DC convertor. However, in case of an emergency such as the failure of on-board power supply, its power supply is provided by the discharge module of magnetically suspended FESS. The measurement unit with eddy current displacement sensors could timely measure the dynamic displacements of FW rotor in both axial and radial directions, and then fed back to the MCU through the signal conditioning module.

The power energy of magnetically suspended FESS is stored as the form of mechanical energy, and it is

$$E = \frac{1}{2} J_e \omega^2 \tag{1}$$

where J_e is the equatorial moment of inertia, and ω is the rotational speed of FW rotor.

The discharged energy of magnetically suspended FESS is

$$\Delta E = \frac{1}{2} J_e \left(\omega_s^2 - \omega_e^2 \right) \tag{2}$$

where ω_s is initial rotational speed, ω_e is end rotational speed.

B. Discharge Principle of Magnetically Suspended FESS

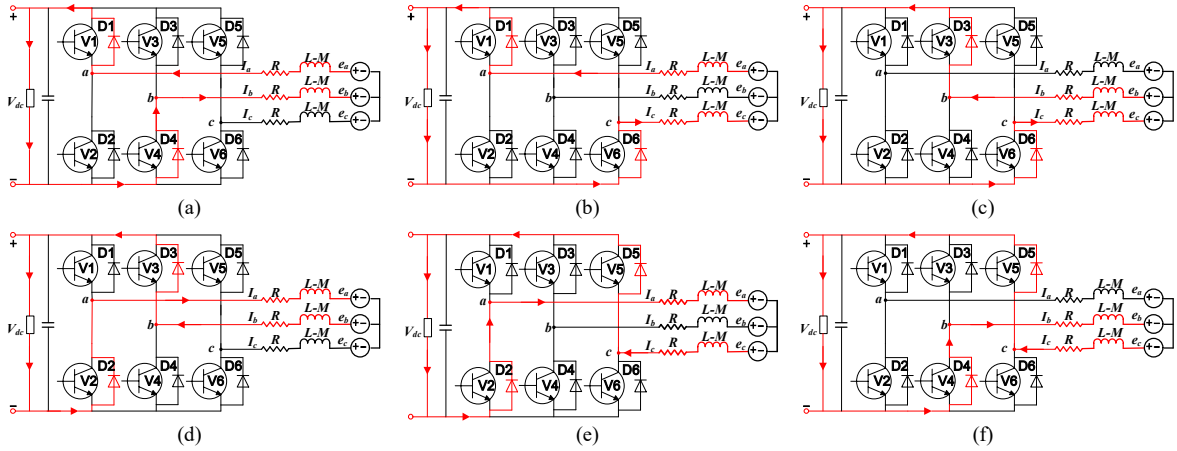

Fig. 3. The rectification process of magnetically suspended FESS.

When the charge/discharge module of magnetically suspended FESS and the control module of AMB system both work normally, the charge module is a motor system to regulate the rotational speed of FW rotor by regulating the *q*-axis control current. If the on-board power supply system of AMB system fails to work, the FW rotor would be worked as a generator to realize the discharge of magnetically suspended FESS.

There are two different operational states for the discharge process of magnetically suspended FESS. When the discharge module works at the passive discharge state, the back EMF of magnetically suspended FESS could be naturally rectified into DC voltage through diodes on three phases. The rectification principle is shown in Fig. 3, and the red line is the current path during the rectification. In the rectification process, all insulated gate bipolar transistors (IGBTs) on three phases are turned off, and the rectification of phase current is realized by controlling turn-on and turn-off of diodes. Therefore, a complete period rectification process is accomplished as six stages with different electrical angles of the FW rotor. For example, in the first stage as illustrated in Fig. 3(a), the voltage at *a*-joint is highest and the voltage at *b*-joint is lowest, so diodes D1 and D4 are turned on. When the electrical angle of FW rotor changes, the current path of rectification would change too.

When the discharge module of magnetically suspended FESS in Fig. 2 works at the active controllable discharge state, the voltage sensors could measure the *q*-axis voltage, and then fed back to the MCU to generate *q*-axis control current through the proportional-integral (PI) controller. In the meanwhile, the phase voltages and phase currents of magnetically suspended FESS are measured to estimate the electrical angle of FW rotor through the SMC model.

Through the *Clark* transform and the *Park* transform, the phase currents I_a and I_b are transformed into the *d*-axis feedback current I_{d_f} and the *q*-axis feedback current I_{q_f}.

Furthermore, the *d*-axis control voltage U_d and the *q*-axis control voltage U_q could be generated through the PI controllers. Through the inverse *Park* transform, the *d*-axis control voltage U_d and the *q*-axis control voltage U_q are converted into the α-axis control voltage U_α and the β-axis control voltage U_β, so the corresponding PWM control signals are generated through the SV switch table terms T_a, T_b and T_c. Finally, the PWM signal could control the turn-on and turn-off of the transistors to realize the controllable rectification of diodes on three phases.

In the feedback loop of discharge module, the *q*-axis and *d*-axis feedback currents are

$$\begin{cases} I_{d\_f} = I_\alpha \cdot \cos\theta_f + I_\beta \cdot \sin\theta_f \\ I_{q\_f} = -I_\alpha \cdot \sin\theta_f + I_\beta \cdot \cos\theta_f \end{cases} \tag{3}$$

where θ_f is the electrical angle of FW rotor, and it is estimated based on the SMC model without measuring the phase voltage.

Based on the inverse *Park* transform, the phase voltages in the control loop are expressed as following

$$\begin{cases} U_\alpha = U_d \cdot \cos\theta_f - U_q \cdot \sin\theta_f \\ U_\beta = -U_d \cdot \sin\theta_f + U_q \cdot \cos\theta_f \end{cases} \tag{4}$$

From the SMC model of electrical angle, we have

$$\begin{cases} \dfrac{di_\alpha}{dt} = -\dfrac{R \cdot i_\alpha}{L_s} + \dfrac{e_\alpha}{L_s} + \dfrac{u_\alpha}{L_s} \\ \dfrac{di_\beta}{dt} = -\dfrac{R \cdot i_\beta}{L_s} + \dfrac{e_\beta}{L_s} + \dfrac{u_\beta}{L_s} \\ e_\alpha = -k_e \omega \sin\theta_f \\ e_\beta = -k_e \omega \cos\theta_f \end{cases} \tag{5}$$

where R is the phase resistance, L_s is the phase inductance, k_e is the back EMF coefficient, e_α and e_β are the back EMF, ω is the rotational speed of the FW rotor.

When the FW rotor works at the rated rotational speed, so

$$\frac{d\omega}{dt} = 0 \tag{6}$$

The back EMF are

$$\begin{cases} \dfrac{de_\alpha}{dt} = -\omega \cdot e_\beta \\ \dfrac{de_\beta}{dt} = -\omega \cdot e_\alpha \end{cases} \tag{7}$$

So the SMC model in (5) could be rewritten into

$$\begin{cases} \dfrac{di_\alpha^0}{dt} = -\dfrac{R \cdot i_\alpha^0}{L_s} + \dfrac{u_\alpha - lz_{e\alpha} - z_\alpha}{L_s} \\ \dfrac{di_\beta^0}{dt} = -\dfrac{R \cdot i_\beta^0}{L_s} + \dfrac{u_\beta - lz_{e\beta} - z_\beta}{L_s} \end{cases} \tag{8}$$

where l is the feedback coefficient, z_α and z_β are the saturation functions of SMC model.

The switch functions of SMC model are

$$\begin{cases} S_\alpha = i_\alpha^0 - i_\alpha \\ S_\beta = i_\beta^0 - i_\beta \end{cases} \tag{9}$$

And then saturation functions of SMC model are

$$\begin{bmatrix} z_\alpha \\ z_\beta \end{bmatrix} = k \cdot sat\left(S_{\alpha\beta}\right) = \begin{cases} k, & S_{\alpha\beta} > \Delta \\ \dfrac{kS}{\Delta}, & -\Delta < S_{\alpha\beta} < \Delta \\ -k, & S_{\alpha\beta} < -\Delta \end{cases} \tag{10}$$

where k is the control parameter of SMC model, the control functions of SMC model are

$$\begin{cases} z_{e\alpha} = \dfrac{z_\alpha \cdot \omega_c}{\left(s + \omega_c\right)} \\ z_{e\beta} = \dfrac{z_\beta \cdot \omega_c}{\left(s + \omega_c\right)} \end{cases} \tag{11}$$

where ω_c is the cutting frequency of low-pass filter. The dynamic functions of SMC observer are

$$\begin{cases} \dfrac{dS_\alpha}{dt} = -\dfrac{R \cdot S_\alpha}{L_s} + \dfrac{u_\alpha - lz_{e\alpha} - z_\alpha}{L_s} \\ \dfrac{dS_\beta}{dt} = -\dfrac{R \cdot S_\beta}{L_s} + \dfrac{u_\beta - lz_{e\beta} - z_\beta}{L_s} \end{cases} \tag{12}$$

If dynamic functions are on the surface of SMC model, there are

$$\begin{cases} S_\alpha = i_\alpha^0 - i_\alpha = 0 \\ S_\beta = i_\beta^0 - i_\beta = 0 \end{cases} \tag{13}$$

Furthermore, there are

$$\begin{cases} e_\alpha = lz_{e\alpha} + z_\alpha \\ e_\beta = lz_{e\beta} + z_\beta \end{cases} \tag{14}$$

Finally, the electrical angle of FW rotor is

$$\theta_f = -\tan^{-1}\left(\frac{e_\alpha}{e_\beta}\right) = -\tan^{-1}\left(\frac{lz_{e\alpha} + z_\alpha}{lz_{e\beta} + z_\beta}\right) \tag{15}$$

For the control loop of q-axis voltage, the error between reference input voltage U_{q_r} and output voltage V_{dc} is

$$e_{q\_u} = U_{q\_r} - V_{dc} \tag{16}$$

Applying the PI controller, the q-axis control current is

$$I_{q\_r} = e_{q\_u} \cdot \left(k_{qu\_p} + k_{qu\_i} \frac{1}{s} \right) \tag{17}$$

Furthermore, the error between the control current and the feedback current is

$$e_{q\_i} = I_{q\_r} - I_{q\_f} \tag{18}$$

Finally, the q-axis control voltage U_q is

$$U_q = e_{q\_i} \cdot \left(k_{qi\_p} + k_{qi\_i} \frac{1}{s} \right) \tag{19}$$

Similarly, the d-axis control voltage U_d is

$$U_d = e_{d\_i} \cdot \left(k_{di\_p} + k_{di\_i} \frac{1}{s} \right) \tag{20}$$

where $e_{d\_i}=I_{d\_r}-I_{d\_f}$. Substituting (19) and (20) into (4), the active rectification of three-phase convertor is realized.

For passive discharge of magnetically suspended FESS, the output DC voltage is

$$V_{dc} = \sqrt{2} \cdot e_{ab} \approx 1.414 \cdot k_e \cdot \omega \tag{21}$$

C. *Converting Module of Output DC Voltage*

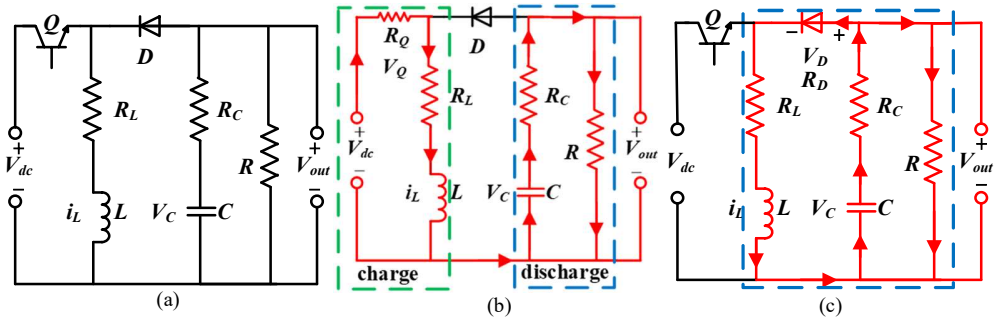

Fig. 4. The Buck-Boost DC/DC convertor, (a) scheme of convertor, (b) turn-on model of transistor, (c) turn-off model of transistor.

The output DC voltage of magnetically suspended FESS is V_{dc}, and the final off-board power supply voltage V_{out} for AMB system is transformed by the Buck-Boost DC/DC convertor as shown in Fig. 4(a). Q is the transistor, R_Q is its equivalent on-resistance, V_Q is its on-voltage. D is the diode, R_D is its on-resistance, V_D is its on-voltage. L is the inductance, R_L is its equivalent resistance. C is the output capacitance, and R_C is its equivalent resistance. R is the load resistance. The current loop of DC/DC convertor is shown in Fig. 4(b) when the transistor Q is turned on, the left loop in green dotted square is the charge loop of input inductance L, and the right loop in blue dotted square is the discharge loop of capacitance C. If the rotational speed of FW rotor is low, the transistor Q is turned off, the DC/DC convertor is then transferred into another loop plotted in Fig. 4(c) with the conducted diode, and then the inductance discharges for load resistance.

Given conditions that V_Q=0 and R_Q=R_C=R_L=0, when the transistor Q is turned on in Fig. 4(b), and the conduction time $\Delta t_{on}=D\cdot T$, where D is the duty ratio and T is period time. The circuit function in Fig. 4(b) is

$$V_{dc} - L\frac{di_L}{dt} - V_{out} = 0 \Rightarrow L \cdot \Delta i_L = \left(V_{dc} - V_{out}\right) \cdot D \cdot T \tag{22}$$

When the transistor Q is turned off in Fig. 4(c), and the turn-off time Δt_{off}=(1-D)·T, so the circuit function is

$$L\frac{di_L}{dt} + V_{out} = 0 \Rightarrow L \cdot \Delta i_L = V_{out} \cdot \left(1 - D\right) \cdot T \tag{23}$$

Combing (22) and (23), there is

$$V_{out} = V_{dc} \cdot D \tag{24}$$

Therefore, the voltage converting of DC/DC convertor could be realized by tuning the duty ratio of transistor's control signal. Similarly, the power supply voltage for AMB system is

$$V_{amb} = V_{out} \cdot N_v \tag{25}$$

where N_v is the voltage transformer ratio.

Furthermore, through different DC/DC converter modules, the output voltage could be transformed into the control voltages of AMB control system including the power voltage of AMB windings (+28V), the power voltage of displacement sensor (+12V) and power voltage of DSP/FPGA chip (+5V).

*D. **Modeling of AMB Winding***

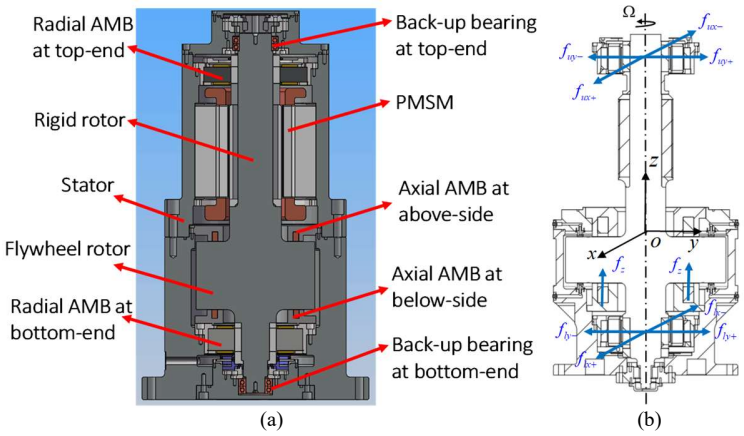

Fig. 5. (a) The structure of magnetically suspended FESS, (b) the force analysis of FW rotor.

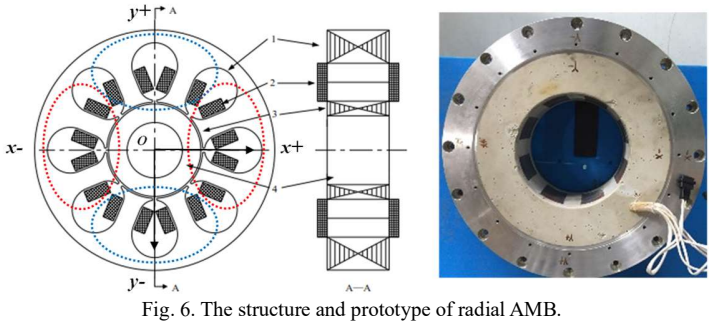

Fig. 6. The structure and prototype of radial AMB.

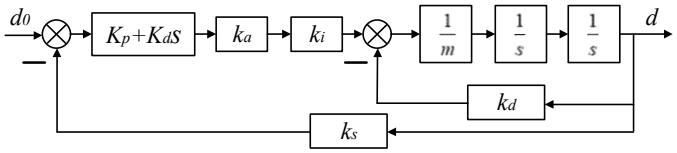

Fig. 7. The control diagram of AMB system.

The structure of magnetically suspended FESS is shown in Fig. 5(a), and it consists of a suspension system, a permanent magnet synchronous motor (PMSM) and a sensor system. The suspension system has two pairs of radial AMBs, two pairs of axial AMB and two pairs of back-up ball bearing. The radial AMB controls the radial motion of FW rotor, and the axial AMB located at above-side and below-side of the FW rotor controls the axial suspension. The back-up ball bearings at top-end and bottom-end secure the stability of FW rotor when the AMB system fails to work or switches off. The PMSM is the drive unit to control the rotation of FW rotor around the axial principal axis. The displacement sensors mounted on the stator part measure radial and axial displacement deflections of FW rotor.

As illustrated in Fig. 5(b), the magnetic forces at top-end and bottom-end hold the FW rotor to work at the radial equilibrium position. The axial magnetic forces generated by the axial AMB hold the FW rotor to suspend at the axial equilibrium position. Considering the gravity of FW rotor, the equations of translation along three axes are

$$\begin{cases} m\ddot{d}_x = f_x \\ m\ddot{d}_y = f_y \\ m\ddot{d}_z = f_z - mg \end{cases} \tag{26}$$

where d_x and d_y are the radial displacements along x and y axis, respectively, and d_z is the axial displacement. f_x, f_y and f_z are the magnetic forces along x, y and z axis, respectively.

The windings of AMB system are driven by the control current. The magnetic force is generated to suspend the FW rotor at the equilibrium point. The structure of radial AMB is shown in Fig. 6. The eight windings are separated into four pairs of control windings, and windings in $x+$ and $x-$ directions are in series connection. The FW rotor is located at inner gap of radial AMB with a controllable airgap to avoid any contact between rotor and stator. Consequently, the magnetic forces along two radial directions (x axis and y axis) control motions of FW rotor.

The magnetic force is assumed to be a linear function of control current and control displacement [30] as following

$$f_{amb} = k_i \cdot i + k_d \cdot d \tag{27}$$

where k_i is the current stiffness, and k_d is the displacement stiffness, and

$$\begin{cases} k_i = \dfrac{\partial f_{amb}}{\partial i} = 2k_{amb} \cdot \dfrac{I_0 + i}{\left(d_0 + d\right)^2} \approx 2k_{amb} \cdot \dfrac{I_0}{d_0^2} \Bigg| \begin{matrix} i = 0 \\ d = 0 \end{matrix} \\ k_d = \dfrac{\partial f_{amb}}{\partial d} = -2k_{amb} \cdot \dfrac{\left(I_0 + i\right)^2}{\left(d_0 + d\right)^3} \approx -2k_{amb} \cdot \dfrac{I_0^2}{d_0^3} \Bigg| \begin{matrix} i = 0 \\ d = 0 \end{matrix} \end{cases} \tag{28}$$

where $k_{amb}=N^2\mu_0 A/4$ is the electromagnetic coefficient, N is the turn's number of winding, A is the cross-sectional area of magnet pole, and μ_0 is the permeability coefficient.

The control diagram of radial AMB in x axis is shown in Fig. 7. k_a is the amplification coefficient, k_s is the sensitivity of the eddy current displacement sensor. Based on the displacement feedback, the control current is

$$i_x=\left(K_P+K_D s\right)k_a k_s\cdot d_x \tag{29}$$

Substituting (29) into (27), the magnetic force is rewritten as

$$f_x=\left(k_{ix}K_P k_a k_s+k_{dx}\right)\cdot d_x+k_{ix}K_D k_a k_s\cdot \dot{d}_x \tag{30}$$

Considering the decoupling among motions in radial and axial directions, the control model of the AMB system in axial direction can be realized too.

III. SIMULATION

A. Charge/Discharge of Magnetically Suspended FESS

The storage power curve of magnetically suspended FESS is plotted in Fig. 8. The blue line is the rotational speed curve of FW rotor, and the red line is the energy storage curve of magnetically suspended FESS, it shows that the storage power varies with the rotational speed. The working status of magnetically suspended FESS could be divided into the charge state and the discharge state. The charge state is realized by accelerating the rotational speed of FW rotor, and the rated storage power is 0.5Kwh with the rotational speed 600rad/s. For the discharge state, the rotational speed of FW rotor is decelerated to the reference value according to defined output power. Referring to different discharge orders, the discharge process is controllable and separated into different stages.

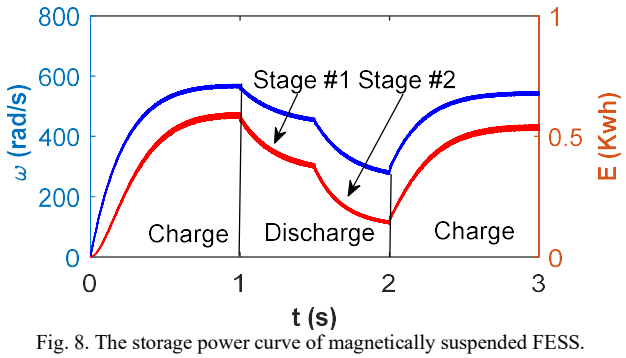

Fig. 8. The storage power curve of magnetically suspended FESS.

B. DC Current and Voltage of Discharge Process

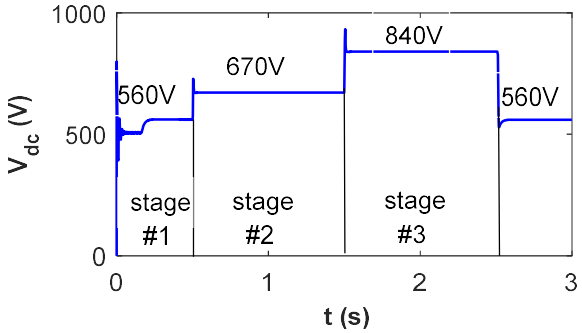

Fig. 9. The output DC voltage of magnetically suspended FESS.

The output DC voltage of magnetically suspended FESS is controllable according to the reference input voltage of rectifier, and the output DC voltage curve with three stages is shown in Fig. 9. In stage 1, the output DC voltage is regulated to the stable reference voltage with set point 560V. The output DC voltage is tuned into 670V at stage 2 with a sudden jump at the setting DC voltage. The output DC voltage is further tuned to the set point with 840V in stage 3. Finally, the output DC voltage drops to the stable reference value at 560V. At this instant, the *d*-axis and *q*-axis currents are illustrated in Fig. 10 during the regulation process of output DC voltage. For the *d*-axis current shown by blue line in Fig. 10(a) and (b), there is obvious jump when the output DC voltage changes to the set point value. For the *q*-axis current plotted by red line in Fig. 10(c) and (d), there is jump value too when the output DC voltage varies.

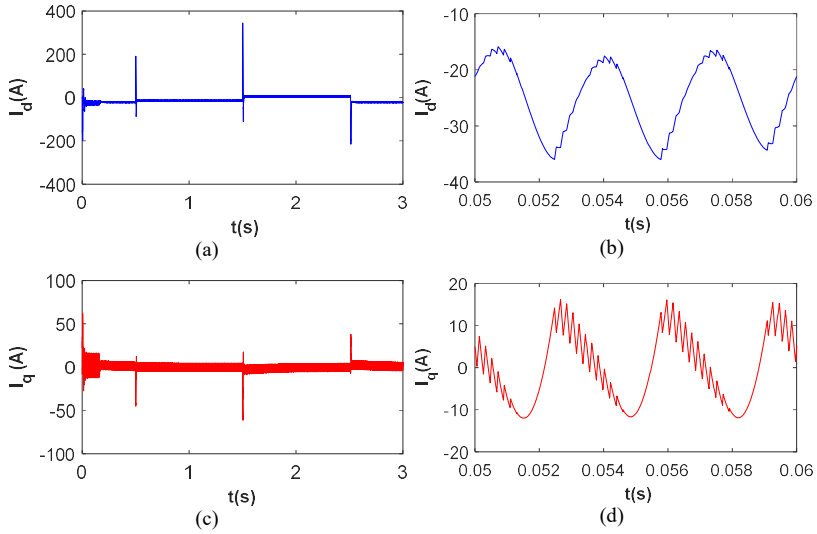

Fig. 10. The *d*-axis and *q*-axis currents of magnetically suspended FESS with variation of output DC voltage, (a) the *d*-axis current during whole process, (b) the *d*-axis current in detail, (c) the *q*-axis current during whole process, (d) the *q*-axis current in detail.

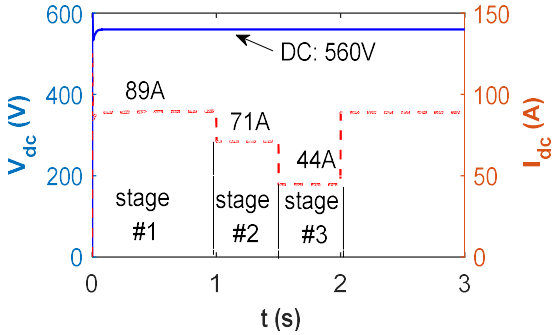

Fig. 11. The output DC current and voltage of magnetically suspended FESS.

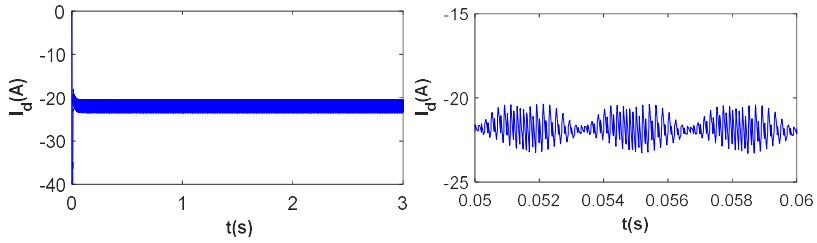

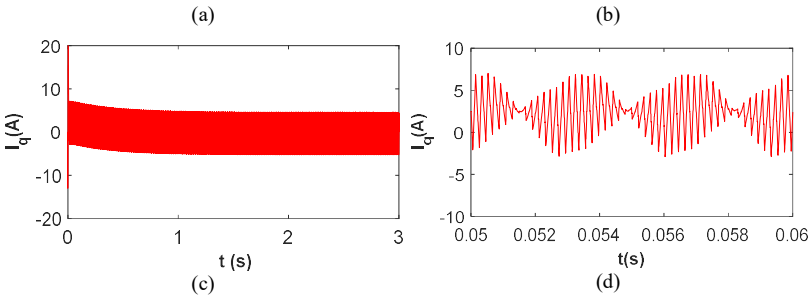

Fig. 12. The *d*-axis and *q*-axis currents of magnetically suspended FESS with variation of load resistance, (a) the *d*-axis current during whole process, (b) the *d*-axis current in detail, (c) the *q*-axis current during whole process, (d) the *q*-axis current in detail.

Moreover, the stable output DC voltage and variation curves of DC current are plotted in Fig. 11. In the discharge process of magnetically suspended FESS, the output DC voltage is always kept at the constant amplitude 560V even the load resistance varies. The response curve of output DC current changing with the variation of load resistance is shown by the red dash line. At stage 1, the load reluctance is about 6.3Ω, and the DC current is 89A. At stage 3, the DC current decreases to 44A when the load resistance increases to 12.5Ω. At this case, the *d*-axis and *q*-axis currents of magnetically suspended FESS with the variation of DC load are plotted in Fig. 12. The *d*-axis and *q*-axis currents keep at a stable amplitude because the output DC voltage keeps at the invariable amplitude during the discharge process of magnetically suspended FESS.

IV. EXPERIMENT

A. Experimental Setup

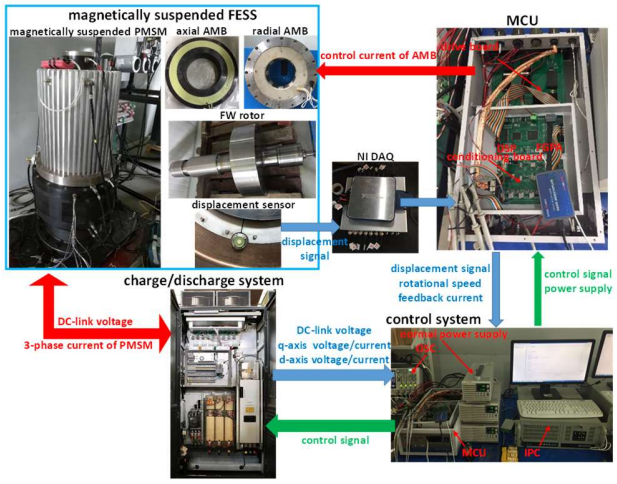

Fig. 13. The whole experimental setup of magnetically suspended FESS.

The whole magnetically suspended FESS in Fig. 13 includes a FESS, an AMB system, a charge/discharge system and an MCU system. The FESS has a PMSM, a rigid FW rotor and a vacuum pump. The PMSM regulates the rotational speed of FW rotor for the charge/discharge process of magnetically suspended FESS, and the vacuum pump could reduce the wind drag of FW rotor at high rotational speed. The charge/discharge module is consisted of six IGBTs, six rectification diodes and a voltage converting system. The IGBTs and rectification diodes form into the

three-phase inverting/rectifying system to realize the charge/discharge of magnetically suspended FESS. The AMB system has four pairs of AMBs, two pairs of AMBs at up-end and low-end are the radial AMB system to control the radial motion and tilting of FW rotor. Two pairs of axial AMBs at up-side and low-side of FW rotor control the axial motion. The MCU system has a DSP/FPGA control board, a NI data acquisition (DAQ) board, a sensor system, and an industrial PC (IPC). The DSP/FPGA control board runs the program of control method, the DAQ board collects system signals such as the dynamic displacements of FW rotor, the rotational speed, the vacuum degree, the phase current of PMSM and the output DC voltage. Above all, the detail parameters of AMB system are listed in TABLE I, and the series number of experimental setups are listed in TABLE II.

TABLE I. PARAMETERS OF AMB SYSTEM

Symbol	Quantity	Value
k_{ai}	axial current stiffness	470 N/A
k_{ad}	axial displacement stiffness	-1700 N/mm
k_{ri}	radial current stiffness	620 N/A
k_{rd}	radial displacement stiffness	-2800 N/mm
k_s	sensitivity of displacement sensor	3.3 V/mm
k_a	amplification coefficient	0.2A/V
K_p	proportional coefficient	5.4
K_d	derivative coefficient	12.8
J_e	equatorial moment of inertia	1.459kgm^2

TABLE II. PARAMETERS OF CHARGE/DISCHARGE SYSTEM

Setup	Series
DAQ Board	NI PCI 6355
DSP	TMS320F28335
FPGA	Altera EPF10K30RC208
FW Rotor	150Kg with 35CrMnSiA
	Density 8000kgm^3
	Poisson ratio 0.3
	Elastic modulus 195GPa
Power Supply	Tektronix Keithley T2231A-30-3
PMSM	Self-designed with 300Kw/5000rpm
Oscilloscope	Keysight 2000 X-Series

B. ***Energy Storage of Magnetically Suspended FESS***

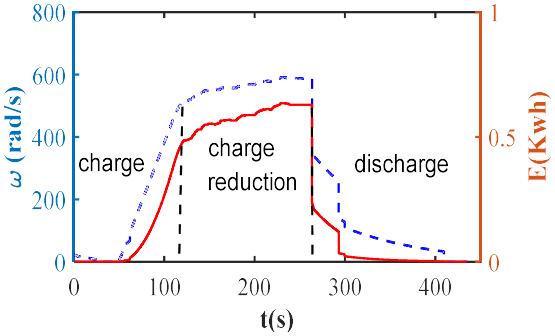

Fig. 14. The energy storage of magnetically suspended FESS.

The energy storage curve of magnetically suspended FESS is illustrated in Fig. 14, the blue dash line is the regulation curve of rotational speed, and the red solid line is the energy storage curve of magnetically suspended FESS. In the charge stage, the energy storage increases with the rotational speed of FW rotor. The energy storage arrives at the saturation state (0.7Kwh) in the charge reduction stage when the rotational speed is at the rated value. In the discharge process, the energy storage quickly drops to the setting value with deceleration of rational speed. So, the magnetically suspended FESS can realize the fast transfer between charge process and discharge process, and then it could restore the power supply of the AMB system by stably outputting DC voltage in the discharge process.

C. ***Charge/Discharge of Magnetically Suspended FESS***

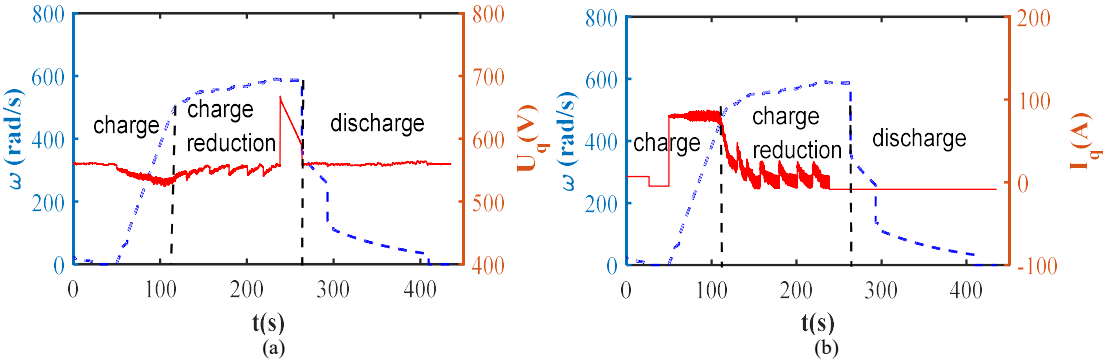

Fig. 15. (a) the *q*-axis voltage of magnetically suspended FESS, (b) The *q*-axis current of magnetically suspended FESS.

In the charge process of magnetically suspended FESS, the input *q*-axis voltage is increased to accelerate the rotational speed of FW rotor, but the *q*-axis voltage is the output DC voltage in the discharge process by decelerating the rotational speed of FW rotor. The relationship between the rotational speed and the *q*-axis voltage is shown in Fig. 15(a). There are three stages including the charge stage, the charge reduction stage (balanced stage) and the discharge stage. The power storage of magnetically suspended FESS increases with the rotational speed of FW rotor in the charge stage, and the *q*-axis voltage remains at a stable value. When the rotational speed of FW rotor approaches to the rated value, the charge stage is changed to the charge reduction stage. In the discharge stage, the rotational speed of FW rotor is decelerated to another rated value, and the magnetically suspended FESS outputs stable DC voltage. In addition, the *q*-axis current in the charge/discharge process is plotted in Fig. 15(b). In the charge stage, the *q*-axis current is

augmented to accelerate the rotational speed of FW rotor so that the energy storage of magnetically suspended FESS increases. When the rotational speed of FW rotor approaches to the rated value, the charge stage is finished and transits to the charge reduction stage, and the rotational speed the FW rotor remains at the rated value. In the discharge stage, the *q*-axis current will be decreased to zero, so the rotational speed of FW rotor decelerates to another rated value.

*D. **Control of AMB System***

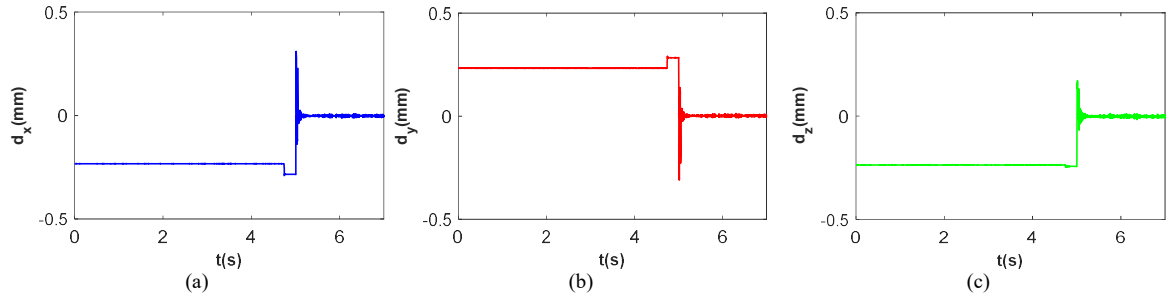

Fig. 16. The Static and dynamic suspension of FW rotor, (a) static suspension in *x* axis, (b) static suspension in *y* axis, (c) static suspension in *z* axis.

The AMB system is used to suspend the FW rotor at the equilibrium point in order to eliminate the friction between the rotor part and the stator part. The dynamic displacements of FW rotor are measured by eddy current displacement sensors in radial and axial directions. As illustrated in Fig. 16(a), (b) and (c), displacement terms d_x, d_y and d_z both equal to zero when the FW rotor is stably suspended at the radial and axial equilibrium positions. Therefore, the experimental result indicates that the AMB system could suspend the FW rotor at the equilibrium point in air and eliminate the friction between the stator part and the rotor part.

*E. **Displacement Deflection of FW Rotor***

In the charge/discharge process of magnetically suspended FESS, the dynamic displacements of FW rotor are plotted in Fig. 17. At the beginning of charge process, the radial displacement deflection of FW rotor is 0.12mm in Fig. 17(a) and (b), and the axial displacement deflection is 0.015mm in Fig. 17(c). When the rotational speed of FW rotor approaches to the rated value, the dynamic displacement of FW rotor approaches to the balanced status, so the displacement deflection of FW rotor is about zero. In the discharge process of magnetically suspended FESS, there is obvious oscillation of radial displacement. The maximum obviation of radial displacement increases to 0.18mm, but the axial displacement deflection keeps at 0.015mm.

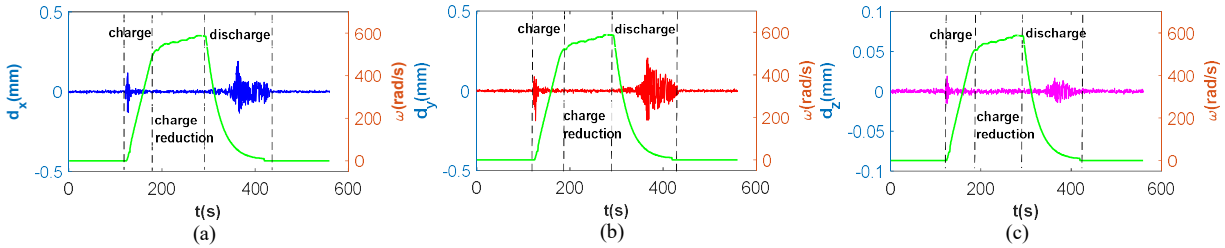

Fig. 17. The dynamic displacements of FW rotor in the charge/discharge process of magnetically suspended FESS, (a) dynamic displacement in *x* axis, (a) dynamic displacement in *y* axis, (a) dynamic displacement in *z* axis.

F. Power Compensation for AMB System

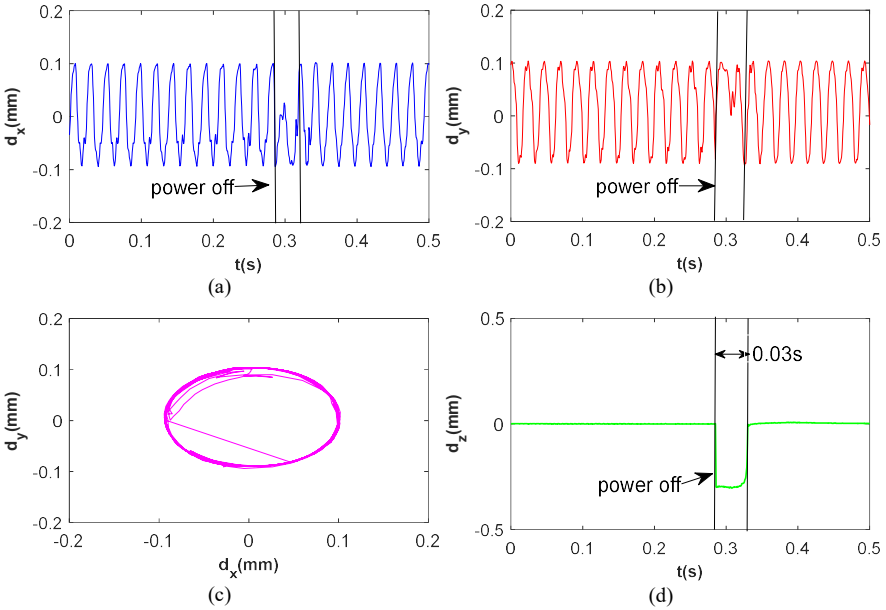

Fig. 18. The dynamic displacements of FW rotor with the power compensation of magnetically suspended FESS, (a) dynamic displacement in *x* axis, (b) dynamic displacement in *y* axis, (a) axis orbit, (a) dynamic displacement in *z* axis.

In the experiment of power compensation mechanism of magnetically suspended FESS, the displacement deflection of FW rotor is used to evaluate the stability status of magnetically suspended FESS. The protective gap of back-up bearing at up-end and low-end is defined as 0.5mm. If the displacement deflection of FW rotor exceeds the protective gap, then the magnetically suspended FESS is at unstable state. The unstable state possibly causes fatal damage to the magnetically suspended FESS. On the other hand, when the displacement deflection of FW rotor is always smaller than the protective gap, the magnetically suspended FESS is maintained at the stable status. In addition, the sudden power failure of AMB system is simulated by switching off the on-board power supply system in the experiment, and the power supply of AMB system is switched from the on-board power supply system to the off-board power supply system through the discharge of magnetically suspended FSSS. Simultaneously, the FW rotor would be quickly braked off by outputting the storage energy in the discharge process.

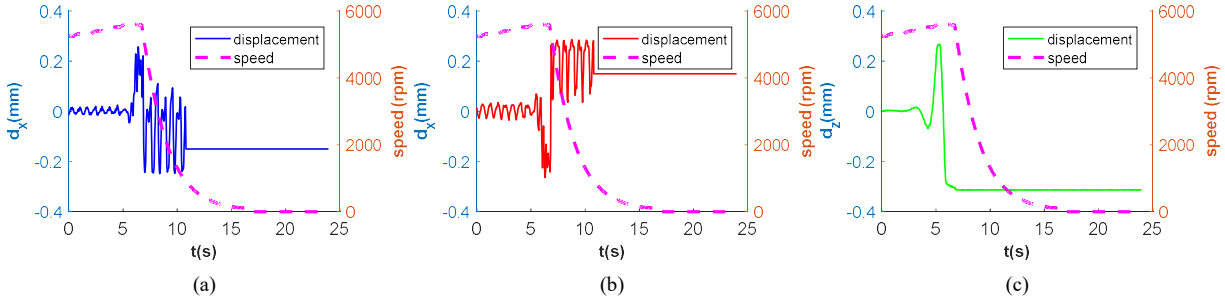

Fig. 19. The dynamic displacements of FW rotor in discharge of magnetically suspended FESS for power compensation, (a) dynamic displacement in *x* axis, (b) dynamic displacement in *y* axis, (a) axis orbit, (a) dynamic displacement in *z* axis.

The dynamic displacements of FW rotor are plotted in Fig. 18 when the rotational speed is 2500rpm. The dynamic displacements of the FW rotor abruptly deflect from the equilibrium point to the unstable location when the on-board power supply system of the AMB system is powered off at t=0.3s. For dynamic displacements of the FW rotor along radial direction in Fig. 18(a) and (b), the stable amplitude is 0.1mm, and displacement deflection is quite small because of the self-center effect of the high-speed FW rotor. For dynamic displacement in axial direction in Fig. 18(d), the displacement deflection is zero when the FW rotor is stably suspended at the axial equilibrium point, and the displacement deflection is 0.3mm when the on-board power supply system of the axial AMB is turned off. With the discharge process of magnetically suspended FESS, the on-board power supply system of AMB system is switched into the off-board power supply system so that the FW rotor is forced back to the axial equilibrium point, and the restore time interval is about 0.03s.

Moreover, the dynamic displacements of FW rotor in discharge of magnetically suspended FESS for power compensation are shown in Fig. 19. The speed of FW rotor is deaccelerated to zero due to the fast discharge. During the deacceleration process of FW rotor, the dynamic displacements have deflection from the equilibrium positions in radial and axial directions, but the deflection values are still restrained in the safe ranges with the magnetic forces of AMB system. Furthermore, the dynamic displacements of FW rotor would be stay at the static values when the speed approaches to zero. Therefore, the protection mechanism of AMB system is realized through the power compensation and the fast deacceleration of magnetically suspended FESS.

Above all, the discharge process of magnetically suspended FESS could timely restore the power failure of the AMB system, and then bring the FW rotor back to the equilibrium point.

V. CONCLUSION AND DISCUSSION

The charge/discharge processes of magnetically suspended FESS are investigated, and the power compensation mechanism of AMB system is successfully realized when the off-board power supply system is provided by the discharge of magnetically suspended FESS. The energy storage of magnetically suspended FESS increases with the rotational speed of the FW rotor, and the discharge process of magnetically suspended FESS is controllable based on the reference DC voltage. More importantly, the power supply system of AMB system is timely substituted by the discharge power of the magnetically suspended FESS if the on-board power supply system fails to work. The proposed backup power system of AMB system can keep the FW rotor working at the equilibrium position so that the damage caused by collision between unstable rotor at high rotational speed and stator can be avoidable.

The power compensation of AMB system is realized by timely discharge of magnetically suspended FESS. However, the switch from the off-board power supply provided by discharge of magnetically suspended FESS to the on-board power supply is not investigated, and it is important to the reliability of power compensation module in this manuscript, so this part of research will be conducted in future.

REFERENCES

[1] H. Liu, J. Jiang, Flywheel energy storage—An upswing technology for energy sustainability, Energy and buildings, 39 (2007) 599-604.

[2] B. Bolund, H. Bernhoff, M. Leijon, Flywheel energy and power storage systems, Renewable and Sustainable Energy Reviews, 11 (2007) 235-258.
[3] A. Kailasan, T. Dimond, P. Allaire, D. Sheffler, Design and analysis of a unique energy storage flywheel system—An integrated flywheel, motor/generator, and magnetic bearing configuration, Journal of Engineering for Gas Turbines and Power, 137 (2015) 042505.
[4] R.S. Weissbach, G.G. Karady, R.G. Farmer, A combined uninterruptible power supply and dynamic voltage compensator using a flywheel energy storage system, IEEE transactions on power delivery, 16 (2001) 265-270.
[5] N. Hamsic, A. Schmelter, A. Mohd, E. Ortjohann, E. Schultze, A. Tuckey, J. Zimmermann, Increasing renewable energy penetration in isolated grids using a flywheel energy storage system, in: 2007 International Conference on Power Engineering, Energy and Electrical Drives, IEEE, 2007, pp. 195-200.
[6] M.I. Daoud, A.M. Massoud, A.S. Abdel-Khalik, A. Elserougi, S. Ahmed, A flywheel energy storage system for fault ride through support of grid-connected VSC HVDC-based offshore wind farms, IEEE Transactions on Power Systems, 31 (2015) 1671-1680.
[7] G.O. Cimuca, C. Saudemont, B. Robyns, M.M. Radulescu, Control and performance evaluation of a flywheel energy-storage system associated to a variable-speed wind generator, IEEE Transactions on Industrial Electronics, 53 (2006) 1074-1085.
[8] H. Akagi, H. Sato, Control and performance of a doubly-fed induction machine intended for a flywheel energy storage system, IEEE Transactions on Power Electronics, 17 (2002) 109-116.
[9] S.M. Lukic, J. Cao, R.C. Bansal, F. Rodriguez, A. Emadi, Energy storage systems for automotive applications, IEEE Transactions on industrial electronics, 55 (2008) 2258-2267.
[10] B.H. Kenny, P.E. Kascak, R. Jansen, T. Dever, W. Santiago, Control of a high-speed flywheel system for energy storage in space applications, IEEE Transactions on Industry Applications, 41 (2005) 1029-1038.
[11] H. Chen, T.N. Cong, W. Yang, C. Tan, Y. Li, Y. Ding, Progress in electrical energy storage system: A critical review, Progress in natural science, 19 (2009) 291-312.
[12] T.D. Nguyen, K.-J. Tseng, S. Zhang, H.T. Nguyen, A novel axial flux permanent-magnet machine for flywheel energy storage system: Design and analysis, IEEE transactions on Industrial Electronics, 58 (2010) 3784-3794.
[13] M. Ahrens, L. Kucera, R. Larsonneur, Performance of a magnetically suspended flywheel energy storage device, IEEE Transactions on control systems technology, 4 (1996) 494-502.
[14] B. Xiang, W. on Wong, Vibration characteristics analysis of magnetically suspended rotor in flywheel energy storage system, Journal of Sound and Vibration, 444 (2019) 235-247.
[15] J. Asama, T. Asami, T. Imakawa, A. Chiba, A. Nakajima, M.A. Rahman, Effects of permanent-magnet passive magnetic bearing on a two-axis actively regulated low-speed bearingless motor, IEEE Transactions on Energy Conversion, 26 (2011) 46-54.
[16] S.E. Mushi, Z. Lin, P.E. Allaire, Design, construction, and modeling of a flexible rotor active magnetic bearing test rig, IEEE/ASME transactions on mechatronics, 17 (2012) 1170-1182.

[17] H. Bleuler, M. Cole, P. Keogh, R. Larsonneur, E. Maslen, Y. Okada, G. Schweitzer, A. Traxler, Magnetic bearings: theory, design, and application to rotating machinery, Springer Science & Business Media, 2009.
[18] J. Tang, B. Liu, J. Fang, S.S. Ge, Suppression of vibration caused by residual unbalance of rotor for magnetically suspended flywheel, Journal of Vibration and Control, 19 (2013) 1962-1979.
[19] J. Fang, S. Zheng, B. Han, AMB vibration control for structural resonance of double-gimbal control moment gyro with high-speed magnetically suspended rotor, IEEE/ASME Transactions on Mechatronics, 18 (2013) 32-43.
[20] J. Tang, K. Wang, B. Xiang, Stable Control of High-Speed Rotor Suspended by Superconducting Magnetic Bearings and Active Magnetic Bearings, IEEE Transactions on Industrial Electronics, 64 (2017) 3319-3328.
[21] S. Lahriri, H.I. Weber, I.F. Santos, H. Hartmann, Rotor–stator contact dynamics using a non-ideal drive—Theoretical and experimental aspects, Journal of Sound and Vibration, 331 (2012) 4518-4536.
[22] B. Xiang, W.o. Wong, Stable control of magnetically suspended motor with heavy self-weight and great moment of inertia, ISA Transactions, (2020).
[23] E. Abele, D. Korff, Avoidance of collision-caused spindle damages—challenges, methods and solutions for high dynamic machine tools, CIRP annals, 60 (2011) 425-428.
[24] O. Grāpis, V. Tamužs, N.-G. Ohlson, J. Andersons, Overcritical high-speed rotor systems, full annular rub and accident, Journal of sound and vibration, 290 (2006) 910-927.
[25] X.-D. Sun, K.-H. Koh, B.-G. Yu, M. Matsui, Fuzzy-logic-based $ V/f $ control of an induction motor for a DC grid power-leveling system using flywheel energy storage equipment, IEEE Transactions on Industrial Electronics, 56 (2009) 3161-3168.
[26] G. Cimuca, S. Breban, M.M. Radulescu, C. Saudemont, B. Robyns, Design and control strategies of an induction-machine-based flywheel energy storage system associated to a variable-speed wind generator, IEEE Transactions on Energy Conversion, 25 (2010) 526-534.
[27] S. Samineni, B.K. Johnson, H.L. Hess, J.D. Law, Modeling and analysis of a flywheel energy storage system for voltage sag correction, IEEE Transactions on Industry Applications, 42 (2006) 42-52.
[28] Q. Cao, Y.-D. Song, J.M. Guerrero, S. Tian, Coordinated control for flywheel energy storage matrix systems for wind farm based on charging/discharging ratio consensus algorithms, IEEE Transactions on Smart Grid, 7 (2015) 1259-1267.
[29] M. Subkhan, M. Komori, New concept for flywheel energy storage system using SMB and PMB, IEEE Transactions on Applied Superconductivity, 21 (2011) 1485-1488.
[30] B. Xiang, W. Wong, Electromagnetic vibration absorber for torsional vibration in high speed rotational machine, Mechanical Systems and Signal Processing, 140 (2020).